applied optics

Reactive dynamics analysis of critical Nb_2O_5 sputtering rate for drum-based metal-like deposition

Shigeng Song, Cheng Li, Hin On Chu, and Des Gibson*

Institute of Thin Films, Sensors & Imaging, SUPA, University of the West of Scotland, Scotland PA1 2BE, UK
**Corresponding author: Des.Gibson@uws.ac.uk*

Received 30 August 2016; revised 9 October 2016; accepted 11 October 2016; posted 11 October 2016 (Doc. ID 274926); published 1 February 2017

Drum-based metal-like film deposition for oxide was investigated using single wavelength *in situ* monitoring. The data were used to investigate the oxidation mechanism using combined second-order kinetic and parabolic models. A critical Nb_2O_5 deposition rate of 0.507 nm/s was found at drum rotation of 1 rev/s. However, Nb_2O_5 samples prepared at varying deposition rates showed that the deposition rate must be much lower than the critical deposition rate to achieve reasonable absorption. Thus simulation for the volume-fraction of metal in the oxide layer was done using effective medium approximation and a distribution function. Simulation gave high agreement with experimental results and allows the prediction of extinction coefficients at various deposition rates.

OCIS codes: (310.1860) Deposition and fabrication; (310.3840) Materials and process characterization; (310.6860) Thin films, optical properties.

https://doi.org/10.1364/AO.56.00C206

1. INTRODUCTION

Plasma oxidation has been widely used in reactive thin film deposition processes. In the system described in this work, substrates were mounted on a rotating drum alternately passing through a sputter deposition area and a microwave oxygen plasma area [1,2]. Target material can be sputtered under metal-like conditions and further oxidized in the microwave plasma area; this allows high deposition rates while increasing the probability of obtaining stoichiometric oxides. It is therefore important to determine how thick a layer of metal can be sufficiently oxidized in one revolution of the drum; this thickness is correlated to the upper limit of the deposition rate for the reactive sputtering system. Sufficiently oxidized film has low absorption, which may enable some particular applications; for example, high-quality coatings with low optical absorption and mechanical loss are currently being developed for gravitation wave detection and high laser damaging threshold application in our institute.

Plasma oxidation of the thin film process involves three parts: plasma gas phase, oxide layer, and substrate. In the plasma gas phase, the species involved in oxidation are possibly O^-, O_2^- ions—atomic O or molecular O_2. It is first supposed, in analogy with conventional wet anodization, that the oxygen ions are mainly responsible for oxidation and originate directly from the oxygen plasma. The results given by Moruzzi *et al.* indicated that O- in the plasma gas phase is responsible for oxidation at lower pressures (0.1 Torr) [3], which fall in thin film process working conditions. When a pure metal surface without a barrier of oxide is exposed to an oxygen-including atmosphere, the oxidation rate usually remains constant with time and the oxidation rate follows a linear model [4]. After a thin oxide barrier has formed, transport mechanisms inside the oxide layer are important for the oxidation process; ion transportation in the oxide layer includes thermal diffusion and field-assisted transports. Field-assisted ion transportation is the main contribution in plasma anodization when the sample has positive potential; however, the thermal diffusion process may be more dominant when the sample has floating potential. The mechanism describing the oxidation kinetics after a very thin oxide layer has formed is the so-called thin film mechanism of oxidation. A range of kinetic models such as the Deal–Grove (DG) model [5], the Massoud model, and the Cabrera–Mott (CM) model [6,7] have been used to describe thin film mechanisms of the surface oxidation process. There are also other oxidation models such as the parabolic model and the logarithmic model [7].

The properties of oxide thin films, such as optical absorption, depend on mechanisms of plasma enhanced oxidation. In general, at room temperatures, only a few-nanometers-thick oxide layer can be formed as the oxide growth is only activated

by thermal diffusion or Mott potential; there is no external field to enhance oxidation. In our drum-based system, samples are held at floating potential, without external applied voltage, which fits the conditions described above.

In this study, the reflectance was obtained *in situ* using single wavelength monitoring during plasma enhanced oxidation on a pre-deposited Nb surface. Then the oxide layer thickness versus plasma treatment time is obtained by fitting the reflectance data and further analyzed using reactive dynamics. It is clear that from the dynamic analysis, film absorption depends on deposition rate. To verify these results from reactive dynamics, N_2O_5 samples were prepared at varying deposition rates, and their transmission data were fitted to obtain the extinction coefficient, k. The k values at various deposition rates were also simulated using effective medium approximation (EMA) and the composite distribution function, and then compared with experimental data for evaluation.

2. EXPERIMENT

The *in situ* investigation of surface oxidation of metal films was carried out in a pulsed-DC sputtering system assisted with microwave plasma (3 KW power) [8,9]. This system is equipped with a single wavelength optical monitoring system and a temperature-stabilized laser diode operating at the wavelength of 670 nm to provide a very stable signal and large signal-to-noise ratio in reflectance mode [1]. The *in situ* reflectance data were recorded once per second at normal incidence angle.

During the investigations of oxidation by optical monitoring, niobium metal films were first deposited onto silicon substrates under 190 sccm of argon gas flow and without microwave plasma assistance. Immediately after deposition of the fresh metal films, 60 sccm of oxygen gas was introduced into the chamber to observe the initial oxidation of the metal film under the argon/oxygen environment, shown in data by reflectance reduction. This equates to a partial pressure of 0.75 mTorr of oxygen in the chamber. Microwave plasma is then started after reflectance data are stable and a further reflectance reduction is observed. The recorded reflectance data against time were then used to calculate the metal thickness and oxide thickness formed on the metal surface using known optical properties of Nb, Nb_2O_5, Si, and SiO_2 (native oxide on Si surface). The complex refractive indices for Nb, Nb_2O_5, Si, and SiO_2 used in this paper are 2.25-3.37i, 2.321-0i, 3.82-0.0145i, and 1.456-0i at 670 nm wavelength, respectively. A schematic diagram of the drum-based sputtering system is shown in Fig. 1. The advantage of this system is the separated sputtering zone (target, only Ar gas input) and oxidation zone (microwave plasma, Ar and O_2 mixture), giving a metal-like sputtering mode for oxides, increasing the deposition rate for accommodating the large coating area of this system, which is about 80 cm diameter and 30 cm width of the drum. For the Nb_2O_5 samples deposited at varying rates, fixed oxygen partial pressure was maintained to give similar conditions to those during the *in situ* monitoring phase of the experiment. Transmittance data of samples were collected and fitted to obtain k values.

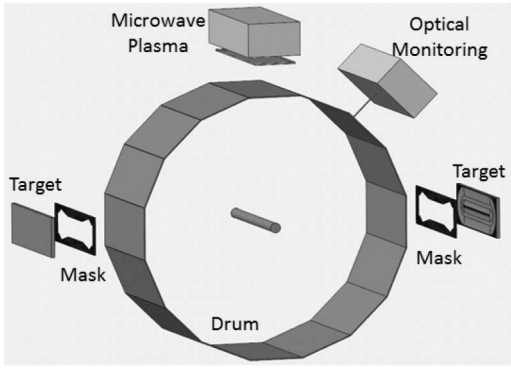

Fig. 1. Schematic diagram of drum-based sputter system with single wavelength *in situ* monitor.

3. MICROWAVE PLASMA ENHANCED SURFACE OXIDATION OF METAL FILM

The measured reflectance during Nb film deposition and oxidation processes is shown in Fig. 2. Reflectance was seen to increase during metal deposition, and reflectance then stabilized in the Ar-only environment after metal deposition was stopped. Once oxygen was introduced to the chamber, reflectance showed a drop, caused by initial oxidation of a pure metal surface. A further drop in reflectance was observed after the microwave plasma started, indicating further oxidation.

The layer stack of oxide layer/metal layer/2-nm-SiO_2/Si substrate was used for optical fitting. The thicknesses of the initial oxidation layer of Nb without plasma were found to be 0.94 nm under 4.75 mTorr total chamber pressure with 0.75 mTorr partial pressure of oxygen in about 100 s. The second drop seen in reflectance data, which was induced by plasma-assisted oxidation, was fitted based on previous deposited Nb metal film. During oxidation, the total Nb atom number in the film must remain the same; thus when the metal film changes to oxide film by oxidation, the thickness of the film will change. The ratio of oxide film to metal film, f, needs to be determined before optical fitting for single wavelength monitoring [2]. The thickness correction factor for Nb to

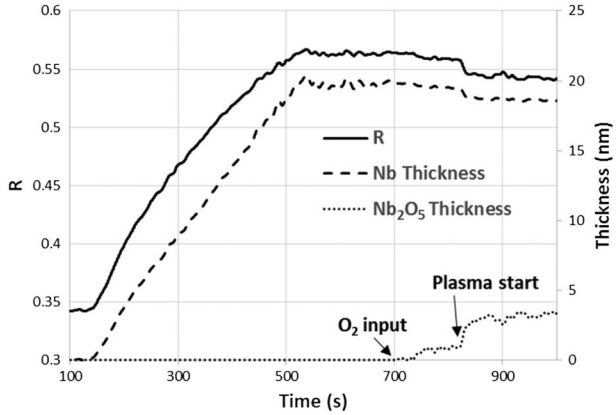

Fig. 2. *In situ* reflectance measurement and resolved Nb and Nb_2O_5 thickness using reflectance versus time, showing Nb_2O_5 thickness increases at O_2 input and plasma start.

Nb_2O_5 is 2.66. Letting the remaining metal thickness after surface oxidation be t, the oxide thickness formed is $f * (t_{metal} - t)$, where f is the thickness correction factor and t_{metal} is the thickness of the metal before oxidation. Programs used for optical fitting were written using Mathcad software. The thickness of the metal and oxide layer against time is also shown in Fig. 2.

4. KINETICS OF MICROWAVE PLASMA ENHANCED OXIDATION

Kinetic models such as the DG model, Massoud model, and CM model have been used to describe thin film mechanisms of surface oxidation processes including thermal oxidation and plasma enhanced oxidation. The linear model and parabolic model can be mathematically derived from the DG model: if the oxide layer is very thin, a linear relation may be obtained; if the oxide layer is thick, a parabolic relation may be obtained. For this investigation, the equations of surface initial oxidation of a pure metal surface, which have been developed by using the kinetics of chemical reaction [2], are also used. The equations are as follows.

For a first-order reaction,

$$d(t) = d_{02}\left[1 - \exp\left(-\frac{t}{\tau}\right)\right] + d_{01}. \quad (1)$$

For a second-order reaction,

$$d(t) = d_{02}\left[1 - \frac{1}{1 + t/\tau}\right] + d_{01}. \quad (2)$$

For convenience, a mathematical function was constructed to cover a wide range of thickness for oxidation data fitting. Oxidation obeys the second-order kinetic model at the start point, and obeys the CM model when a thicker oxide layer has formed. There is a possibility to combine these two models to cover both ranges of the start point oxidation and field-assisted oxidation (CM model). However, an analytical solution cannot be obtained using the CM model; additionally, the growth rate of the CM model tends to infinity when the thickness tends to zero. It is, however, also seen that the parabolic model is widely used for oxidation analysis for thick oxide layers. Therefore, the second-order kinetic model and parabolic model were combined to analyze the experimental data using the following equation:

$$d(t) = d_1\left[1 - \frac{1}{1 + t/\tau}\right] + d_2 \cdot t^{1/2}, \quad (3)$$

where $d(t)$ is the thickness at time t, τ is the time constant, d_1 is the final thickness of the initial oxide layer, and d_2 is the parabolic growth constant. Dimensions for t and τ are in seconds, for d_1 and $d(t)$ are in nanometers, and for d_2 are in $nm/s^{1/2}$. As it is difficult to determine the exact start time of oxidation, an extra parameter, time offset t_0, is used for experimental data fitting. Experimental data (Fig. 2) have shown that plasma-assisted oxidation is the dominant oxidation step. Thus only the data of oxide growth during plasma treatment were fitted. The results are shown in Fig. 3. The fitting parameters of d_1, d_2, and τ are found to be 3.05 nm, 0.053 $nm/s^{1/2}$, and 5.714 s, respectively.

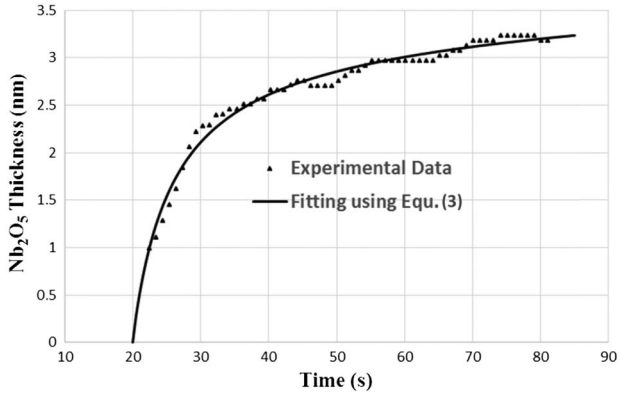

Fig. 3. Thickness fitting for plasma enhanced oxidation using the combined second-order kinetic model and parabolic model, Eq. (3).

Using the fitting results above, the critical deposition rate for our deposition system was determined. The rotation speed of the sputter drum is 60 rpm, and the critical metal thickness for sufficient oxidation in one rotation of the drum (1 s per revolution) was found using Eq. (3): the critical deposition rate of Nb_2O_5 is 0.507 nm in 1 s.

To evaluate and validate this fitted result and to investigate the effect of deposition rate on the extinction coefficient, several N_2O_5 samples were deposited using varying rates. They were then analyzed using transmission spectra, which were then fitted to obtain the reflective index (n) and the extinction coefficient (k). Figure 4 shows an example of transmission fitting of one sample deposited at 0.32 nm/s rate; Fig. 5 shows the changing k due to the varied deposition rate of Nb_2O_5 and is zoomed onto a small wavelength range for better clarity.

The k values for samples with deposition rates 0.32, 0.24, 0.20, 0.15, 0.11, and 0.02 nm/s are 4.30×10^{-4}, 3.03×10^{-4}, 2.33×10^{-4}, 1.74×10^{-4}, 1.44×10^{-4}, and 0.67×10^{-4}, respectively (at wavelength 400 nm). The k value is seen to increase more rapidly when the deposition rate is higher than 0.15 nm/s. There is a large discrepancy from a critical deposition rate of 0.507 nm. This may be due to the optical fitting of the oxide layer thickness using equivalent thickness, assuming a perfectly

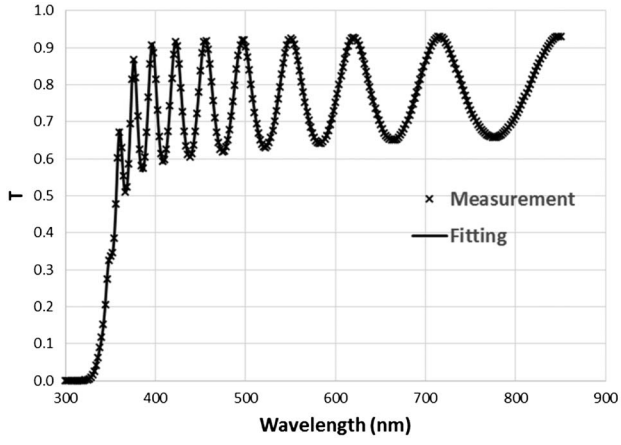

Fig. 4. Transmission fitting of the Nb_2O_5 sample with 0.32 nm/s rate.

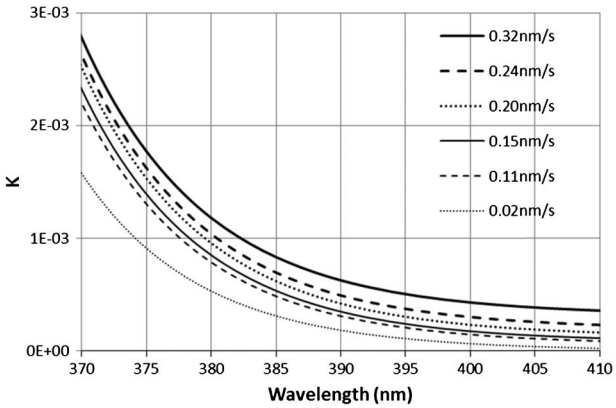

Fig. 5. k values of Nb_2O_5 samples at various deposition rates.

uniform oxide layer. However, oxygen atoms can diffuse inside of the coating and obey the diffusion model; there would be a distribution of oxidation extent inside the oxide layer, resulting in a non-oxidized metal atom in the oxide layer. Detailed discussion appears in Section 5.

5. SIMULATION OF ABSORPTION AGAINST DEPOSITION RATE

A. k Value and Volume Fraction

Section 4 shows the experimental data of k values against deposition rates. For further evaluation and comparison, a simulation of the relations between k values and deposition rates was obtained using the oxidation model.

Due the separated regions of the processes, there is some level of non-fully oxidized metal atoms in the oxide layer. This can be treated as a mixture (composite material) of metal and stoichiometric oxide, and EMA can be used for calculating the dielectric property of this mixture. Bruggeman's model was used for the EMA calculations [10]. The volume fraction of metal in the oxide layer is then found from k values from the below derivations:

$$(1-f)\cdot\frac{\varepsilon_m-\varepsilon_{\text{eff}}}{\varepsilon_m+2\cdot\varepsilon_{\text{eff}}}+f\cdot\frac{\varepsilon_p-\varepsilon_{\text{eff}}}{\varepsilon_p+2\cdot\varepsilon_{\text{eff}}}=0. \quad (4)$$

Here ε_m is the oxide dielectric constant, ε_p is the metal dielectric constant, and ε_{eff} is the effective dielectric constant. f is the metal volume fraction. As the film is nearly stoichiometric oxide, f tends to 0.

Based on Figs. 4 and 5, k values at 400 nm are chosen for modeling as these k values are high and around the absorption edge. The complex refractive indices are 2.5-0i and 1.5-2.99i for Nb_2O_5 and Nb metal at 400 nm, respectively.

Using the approximation of $f\to 0$, and the relation of refractive index and dielectric constant $\varepsilon=n^2$, the effective refractive index of the mixture against the metal volume fraction is obtained (as the equation is quite long, a detailed deduction is not shown here):

$$n_{\text{eff}}(f)\approx 2.500+0.173\cdot f-5.522\cdot f\cdot i. \quad (5)$$

Thus the volume fraction can be obtained using the k value:

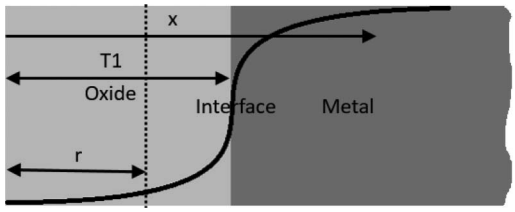

Fig. 6. Distribution of oxidation extent; r is the thickness deposited in 1 s; T1 is the thickness that can be oxidized during 1 s under oxygen microwave plasma.

$$f\approx\frac{k}{5.522}. \quad (6)$$

Therefore the metal volume fractions of samples at deposition rates of 0.32, 0.24, 0.20, 0.15, 0.11, and 0.02 nm/s are 7.79×10^{-5}, 5.49×10^{-5}, 4.22×10^{-5}, 3.15×10^{-5}, 2.61×10^{-5}, and 1.21×10^{-5}, respectively.

B. Distribution Profile and Volume Fraction

Equation (3) in Section 4 describes the equivalent oxide thickness against time. To find the volume fraction of metal, the distribution profile at a certain time is needed—time is 1 s as drum rotation is 1 rev/s. As the oxide layer grows, there is a sharp interface between the oxide and metal layer, as shown in Fig. 6. Assuming the distance from the oxide surface to the interface is T1 for 1 s plasma oxidation and concentration at the interface is 50%, the distribution function was obtained using the exponential distribution of metal atoms in the oxide layer:

$$\rho(x)=\frac{1}{2}\cdot e^{-C1\cdot(T1-x)}. \quad (7)$$

In Eq. (7), T1 is related to the equivalent thickness for 1 s plasma oxidation found by Eq. (3). However, a perfect oxide layer is used for optical fitting in Eq. (3); thus the T1 value is larger than the equivalent thickness when considering the distribution function.

For the continuous deposition process, the average concentration of metal (average volume fraction) needs to be found over the thickness deposited in 1 s (r, deposition rate); the relation between the deposition rate and the average volume fraction is

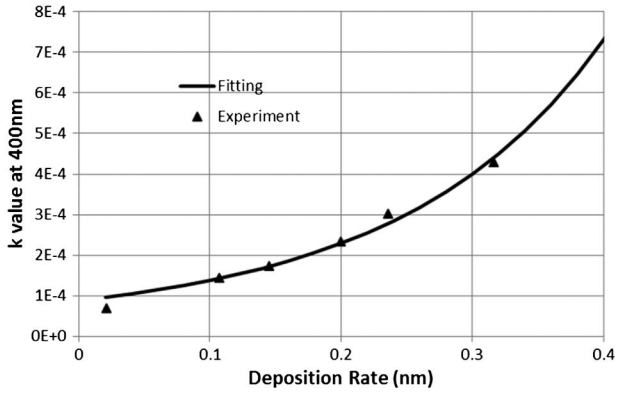

Fig. 7. Relation between k value and deposition rate r. Dots, experimental data; line, simulation data using Eq. (9).

$$f(r) = \frac{1}{(2 \cdot r)} \cdot \int_0^r e^{-C1 \cdot (T1 - x)} \cdot dx. \quad (8)$$

Finally, combining Eqs. (5) and (8), the relation between the k value and the deposition rate r is obtained. Figure 7 shows the fitting results using Eq. (9) ($C1 = 8.42$ nm^{-1} and $T1 = 1.23$ nm). Good agreement is shown between simulation and experimental data:

$$k(r) = 2.761 \cdot e^{-C1 \cdot T1} \cdot (e^{-C1 \cdot r} - 1)/(C1 \cdot r). \quad (9)$$

6. CONCLUSIONS

A drum-based metal-like film deposition for oxide was investigated using single wavelength *in situ* monitoring. The reactive oxide deposition undergoes two processes: metal deposition and plasma enhanced oxidation, in their respective regions. Single wavelength *in situ* monitoring investigation was carried out to analyze the oxide thickness growth mechanism using combined second-order kinetic and parabolic models. *In situ* monitoring data were fitted with known optical parameters and measured thickness to obtain a critical deposition rate of Nb_2O_5:0.507 nm/s for 1 rev/s drum rotation. To evaluate and validate this critical deposition rate and to investigate the effect of deposition rate on the extinction coefficient, several N_2O_5 samples were deposited at varying deposition rates.

However, it was then observed that the deposition rate must be much lower than the critical deposition rate in order to achieve reasonably low absorption. To understand and predicate absorption dependence on deposition rate for such a drum-based system, EMA (Bruggeman's model) and the distribution function are used to simulate the volume fraction of metal in the oxide layer. The simulation agrees well with the experimental relation between k and the deposition rate. This developed method can also be used to predicate the extinction coefficients, k, at a various deposition rates and to ensure the desired oxidation extent.

Funding. Biotechnology and Biological Sciences Research Council (BBSRC) (BB/P005020/1).

REFERENCES

1. S. Song and F. Placido, "*In-situ* investigation of spontaneous and plasma-enhanced oxidation of AlN film surfaces," Appl. Phys. Lett. **99**, 121901 (2011).
2. S. Song and F. Placido, "Investigation on initial oxidation kinetics of Al, Ni, and Hf metal film surfaces," Chin. Opt. Lett. **8**, 87–90 (2010).
3. J. L. Moruzzi, A. Kiermasz, and W. Eccleston, "Plasma oxidation of silicon," Plasma Phys. **24**, 605–614 (1982).
4. J. R. Davis, *Heat-Resistant Materials* (ASM International, 1997).
5. S. A. Campbell, *The Science and Engineering of Microelectronic Fabrication* (Oxford University, 1996).
6. N. Cabrera and N. Mott, "Theory of the oxidation of metal," Rep. Prog. Phys. **12**, 163–184 (1984).
7. V. P. Parkhuttik, "Modelling of low temperature oxidation of materials in gaseous environments," J. Phys. D **25**, 256–261 (1992).
8. S. Moh and F. Placido, "Microwave-assisted DC magnetron sputtering," in *47th SVC Annual Technical Conference* (2004), p. 443.
9. F. Placido and A. Voronov, "Characterisation of thin metal films of niobium and zirconium," in *47th SVC Annual Technical Conference* (2002), p. 266.
10. D. A. G. Bruggeman, "Berechnung verschiedener physikalischer Konstanten von heterogenen Systemen," Ann. Phys. **416**, 665–679 (1935).